Bound vector solitons and soliton complexes for the coupled nonlinear Schrödinger equations

Zhi-Yuan Sun,[1] Yi-Tian Gao,[1,2,*] Xin Yu,[1] Wen-Jun Liu,[3] and Ying Liu[1]
[1]*Ministry-of-Education Key Laboratory of Fluid Mechanics and National Laboratory for Computational Fluid Dynamics, Beijing University of Aeronautics and Astronautics, Beijing 100191, China*
[2]*State Key Laboratory of Software Development Environment, Beijing University of Aeronautics and Astronautics, Beijing 100191, China*
[3]*School of Science, Beijing University of Posts and Telecommunications, P.O. Box 122, Beijing 100876, China*
(Received 22 July 2009; revised manuscript received 12 November 2009; published 31 December 2009)

Dynamic features describing the collisions of the bound vector solitons and soliton complexes are investigated for the coupled nonlinear Schrödinger (CNLS) equations, which model the propagation of the multimode soliton pulses under some physical situations in nonlinear fiber optics. Equations of such type have also been seen in water waves and plasmas. By the appropriate choices of the arbitrary parameters for the multisoliton solutions derived through the Hirota bilinear method, the periodic structures along the propagation are classified according to the relative relations of the real wave numbers. Furthermore, parameters are shown to control the intensity distributions and interaction patterns for the bound vector solitons and soliton complexes. Transformations of the soliton types (shape changing with intensity redistribution) during the collisions of those stationary structures with the regular one soliton are discussed, in which a class of inelastic properties is involved. Discussions could be expected to be helpful in interpreting such structures in the multimode nonlinear fiber optics and equally applied to other systems governed by the CNLS equations, e.g., the plasma physics and Bose-Einstein condensates.

DOI: 10.1103/PhysRevE.80.066608 PACS number(s): 05.45.Yv, 42.65.Tg, 42.81.Dp

I. INTRODUCTION

In such fields as fluids, plasmas, and fiber communication systems, the nonlinear evolution equations (NLEEs), with their soliton solutions, appear as good models [1–4].

The optical soliton used as the carrier of the information bits is one of the robust subjects since it has the ability to propagate over long distances without losing its identities, which is a property due to the balance between the self-phase modulation (SPM) and dispersion effects [1,5,6]. The basic models describing the propagation of the picosecond pulses (temporal solitons) in single-mode fibers are governed by the nonlinear Schrödinger (NLS)-typed equations, including the higher-order NLS equations for the femtosecond pulses [1,4,7], which are a typical type of the NLEEs. In order to increase the transmission capacity of the lightwave systems, it is necessary to consider the cases of the wavelength division multiplexing (WDM) [8] and multichannel bit-parallel-wavelength optical fiber networks [9], where the pulses propagate at least in two channels simultaneously [1,10]. In those systems, the coupled NLS (CNLS) equations, which model the propagation of the multimode soliton pulses, are of current interest and extensively discussed [6,11–14]. In fact, the use of massive WDM systems is enabled by the fiber amplifiers and has led to the development of the lightwave systems with the capacities exceeding 1 Tb/s [1]. Besides, the CNLS equations arise in a variety of scientific areas such as the biophysics, Bose-Einstein condensates (BECs), plasma physics, and two-wave systems in both shallow and deep waters [13–20].

Different from the single NLS-typed equations, the CNLS equations support the vector solitons, a composite structure with two (or more) components (modes) that mutually self-trap in a nonlinear medium [21]. Such concept was first suggested in Ref. [22] as considering the orthogonally polarized components in the nonlinear Kerr medium, where the SPM is identical to the cross-phase modulation (XPM). Those vector structures have also appeared in the dynamics of two nonlinear coupled waves (laser beams) in the plasmas [18,19]. The collisions of the vector solitons have some unique features and become one of the frequently investigated phenomena [21,23]. Two different multimode solitons can be generated from the collision process through the shape transformation [13,21], and associated with such transformation, one feature is the energy exchange between the components of the colliding vector solitons with the intensity redistribution [6,13,21,23,24]. Further studies demonstrate that the energy redistribution can be efficiently controlled by an appropriate choice of the initial physical conditions [23]. In those references devoting to the shape transformation (energy redistribution), two categories of the methods have been used in general: one being the numerical procedure based on the split-step Fourier (SSF) method [23], the other based on the analytical solutions obtained with the Hirota bilinear method [6,13,24]. As experimental supports, the collision behaviors have also been observed in the birefringent fibers [25] and photorefractive media [26]. With those properties, the collisions of the vector solitons provide applications in the areas of the collision-based logic gates and optical computation [13,25,27].

The regular vector multisolitons can separate before or after collisions and propagate as the independent individuals [6]. Specially, two adjacent vector solitons could form a bound state, which confines the soliton motions in the stationary regions [21]. With more complex collision patterns, such bound vector solitons have attracted much attention [28–31]. In Ref. [28], analytic and numerical studies of the CNLS equations reveal the existence of a class of bound

*Corresponding author; gaoyt@public.bta.net.cn

vector solitary waves without interactions, which suggests the possibility of reducing soliton interactions in the optical fiber transmission systems. Correspondingly, for the CNLS equations, a periodic rotation or beating of the polarization state and a periodic coalescence between the two in-phase (the relative phase is zero) polarization components of the pulses have been observed through numerical simulations [29]. As mentioned above, the collisions of the vector solitons have certain unique features, which is not an exception for those of the bound vector solitons [21,30,31]. Compared with the scalar solitons governed by the single NLS equation, the existence of the stationary bound states for the dark-type vector solitons in the isotropic Kerr-type media is a novel phenomenon [30], while another different feature emphasizes that the vector solitons in the two-vector-bound states repel or attract each other, depending not only on their relative phases but also on their initial position separation [31].

On the other hand, the multisoliton complex, viewed as a localized superposition of the fundamental solitons, has been studied for its sophisticated dynamic properties [6,12,13,32–35]. Those fundamental solitons interact both coherently and incoherently [32], while the soliton complex is able to show the variable profile and shape variation in the moving and colliding process [13]. Some spatial soliton structures can be attributed to the special cases of the multisoliton complexes, such as the incoherent soliton [32] and partially coherent soliton (PCS) [12,13]. The experimental research on the collision of the one-dimensional PCS in the photorefractive crystal has been provided in Ref. [33]. Recently, the analytic investigation of the CNLS equations with the Hirota bilinear method indicates that some multisoliton complexes (e.g., PCS) have close connections with the regular multisoliton solutions with respect to their collision processes [6,13]. Under those circumstances, the variation in the shape of the PCS has been explained as the result of the intensity redistribution of the fundamental solitons during the collision, and such interpretation offers an effective way to understand the relevant phenomenon [6,13]. Furthermore, the scenario of the energy redistribution may have potential value to explain the shape changing of the bound vector solitons or other complex structures.

Hereby investigated in this paper are the bound vector solitons and soliton complexes for the following integrable CNLS equations [6,11,12,14,24]:

$$iq_{1,z} + q_{1,tt} + 2\mu(|q_1|^2 + |q_2|^2)q_1 = 0, \tag{1a}$$

$$iq_{2,z} + q_{2,tt} + 2\mu(|q_1|^2 + |q_2|^2)q_2 = 0, \tag{1b}$$

where q_1 and q_2 are the slowly varying envelopes of the two interacting optical modes, z and t represent the normalized distance along the direction of the propagation and the retarded time (Note that when the spatial solitons are discussed, t can be replaced by x, the transverse coordinate), and 2μ gives the strength of the nonlinearity. Equations (1) have been studied as the ones of the Manakov type with the XPM coefficient equating one [11]. The NLEEs of such type have also been investigated with respect to the modulational instability of the coupled nonlinear waves in water waves and plasmas [17–19]

With the aid of the Hirota bilinear method [36], the analytic bright-bright multisolitons for Eqs. (1) have been derived and investigated on the aforementioned shape transformation with the intensity redistribution [6,11–14,24]. Here one of the advantages by using the Hirota bilinear method is that it permits six arbitrary complex parameters to control the amplitude, phase shift, pulse width, and relative separation distance during the collisions of the regular vector solitons [14,24,37].

However, to our knowledge, the present interest on Eqs. (1) has mainly been focused on the collisions of the regular multisolitons derived explicitly from the Hirota bilinear method [6,11,13,24] but ignoring its ability to provide more complicated structures, e.g., the bound solitons and soliton complexes. On the other hand, those stationary structures, associated with their interactions, are usually discussed as various independent individuals [12,13,29,30,33–35], lacking of the internal connections among them. Moreover, we believe that it is necessary to investigate the following two questions: (i) how the energy is redistributed in the collision of those stationary structures; (ii) whether certain principles for the shape changing of the regular multisolitons are appropriate to explain the confined interaction patterns.

With above considerations, in Secs. II and III of this paper, we will demonstrate the evolution from the periodic bound vector solitons to a class of soliton complexes through gradually changing the relative relations of the two real wave numbers for the two-soliton solutions derived by the Hirota bilinear method. Some of those complicated solitons can be viewed as the new structures for Eqs. (1). Numerical simulations have also been performed to support the analytical results. Section IV will ulteriorly discuss the intensity distribution of the bound vector solitons and soliton complexes by controlling the free parameters in the analytical solutions. In Sec. V, we discover that during the collisions between those stationary structures and the regular one soliton, there exist two types of collision patterns in general: (i) the transformation among the basic types of those stationary structures according to our classification; (ii) the increase or decrease in the asymmetry for the stationary structures, but without the transformation of the basic soliton patterns. In addition, several inelastic properties will be referred in each section, which can benefit the understanding of the existed phenomena in the nonlinear fiber optics and plasma physics or provide relevant applications in those fields.

II. INTEGRALS OF MOTION AND BILINEAR FORMS

Two integrals of motion for Eqs. (1), the energy E and the linear momentum M of the pulses, are given by Ref. [10] as

$$E = \int_{-\infty}^{\infty} (|q_1|^2 + |q_2|^2)dt, \tag{2}$$

$$M = i\int_{-\infty}^{\infty} (q_1^* q_{1,t} - q_1 q_{1,t}^* + q_2^* q_{2,t} - q_2 q_{2,t}^*)dt, \tag{3}$$

where $*$ denotes the complex conjugate. Equation (2) implies the conservation of the total energy for the two modes. Such

conservation is a general principle in both situations including the intensity redistribution (enhancement and suppression) in each single mode and the energy switching between the two modes.

The explicit expressions of the bight-bright vector solitons for Eqs. (1) have been obtained by the Hirota bilinear method [11,13,24,37]. By using the transformations

$$q_1 = \frac{g}{f}, \quad q_2 = \frac{h}{f}, \tag{4}$$

the bilinear form of Eqs. (1) can be derived as

$$(iD_z + D_t^2) g \cdot f = 0, \quad (iD_z + D_t^2) h \cdot f = 0,$$
$$D_t^2 f \cdot f = 2\mu(gg^* + hh^*), \tag{5}$$

where $f(z,t)$ is a real function, $g(z,t)$ and $h(z,t)$ are complex functions, and the Hirota's bilinear operators are defined by [36]

$$D_z^n D_t^m a \cdot b = \left(\frac{\partial}{\partial z} - \frac{\partial}{\partial z'}\right)^n \left(\frac{\partial}{\partial t} - \frac{\partial}{\partial t'}\right)^m a(z,t) b(z',t')|_{z=z',t=t'}. \tag{6}$$

By applying the method of the formal parameter expansion, the two-soliton solutions can be obtained as [24]

$$q_j = \frac{\alpha_1^{(j)} e^{\eta_1} + \alpha_2^{(j)} e^{\eta_2} + e^{\eta_1+\eta_1^*+\eta_2+\delta_{1j}} + e^{\eta_1+\eta_2+\eta_2^*+\delta_{2j}}}{1 + e^{\eta_1+\eta_1^*+R_1} + e^{\eta_1+\eta_2^*+\delta_0} + e^{\eta_1^*+\eta_2+\delta_0^*} + e^{\eta_2+\eta_2^*+R_2} + e^{\eta_1+\eta_1^*+\eta_2+\eta_2^*+R_3}}, \quad j = 1,2, \tag{7}$$

where

$$\eta_j = k_j(t + ik_j z),$$

$$e^{\delta_0} = \frac{\kappa_{12}}{k_1 + k_2^*}, \quad e^{R_1} = \frac{\kappa_{11}}{k_1 + k_1^*}, \quad e^{R_2} = \frac{\kappa_{22}}{k_2 + k_2^*},$$

$$e^{\delta_{1j}} = \frac{(k_1 - k_2)(\alpha_1^{(j)}\kappa_{21} - \alpha_2^{(j)}\kappa_{11})}{(k_1 + k_1^*)(k_1^* + k_2)},$$
$$e^{\delta_{2j}} = \frac{(k_2 - k_1)(\alpha_2^{(j)}\kappa_{12} - \alpha_1^{(j)}\kappa_{22})}{(k_2 + k_2^*)(k_1 + k_2^*)}, \tag{8a}$$

$$e^{R_3} = \frac{|k_1 - k_2|^2}{(k_1 + k_1^*)(k_2 + k_2^*)|k_1 + k_2^*|^2}(\kappa_{11}\kappa_{22} - \kappa_{12}\kappa_{21}), \tag{8b}$$

$$\kappa_{jl} = \frac{\mu(\alpha_j^{(1)}\alpha_l^{(1)*} + \alpha_j^{(2)}\alpha_l^{(2)*})}{k_j + k_l^*}, \quad j,l = 1,2. \tag{8c}$$

Solution (7) is characterized by six arbitrary complex parameters including the wave numbers k_1, k_2 and four parameters $\alpha_1^{(j)}$, $\alpha_2^{(j)}$, $j=1,2$. For the two modes of both regular solitons during collision, the special case $\alpha_1^{(1)}/\alpha_2^{(1)} = \alpha_1^{(2)}/\alpha_2^{(2)}$ does give the standard elastic collision; otherwise, the inelastic collision occurs [13]. If the two wave numbers are confined to be some selected real numbers, the collision structures that differ from the regular two-soliton solutions, i.e., the bound vector solitons as well as the soliton complexes, can be derived from those explicit algebraic expressions. The details will be presented in the following sections.

III. BASIC BOUND VECTOR SOLITONS AND SOLITON COMPLEXES WITH BRIEF NUMERICAL SIMULATIONS

Without loss of generality, we assume that $\mu=1$, $\alpha_1^{(j)} = \alpha_2^{(j)} = 1$, $j=1,2$, and focus on the relationship between the real wave numbers k_1 and k_2. Under such assumptions, Solution (7) can be rewritten through symbolic computation [2–4] as

$$q_j = \frac{e^{\eta_1} Q_1 + e^{\eta_2} Q_2}{2D k_1^2 k_2^2 (k_1 + k_2)^2}, \quad j = 1,2, \tag{9}$$

where

$$Q_1 = k_1^2[e^{2k_2 t}(k_1 - k_2)^2 + 2k_2^2(k_1 + k_2)^2], \tag{10a}$$

$$Q_2 = k_2^2[e^{2k_1 t}(k_1 - k_2)^2 + 2k_1^2(k_1 + k_2)^2], \tag{10b}$$

$$D = 1 + \frac{e^{2k_1 t}}{2k_1^2} + \frac{e^{2k_2 t}}{2k_2^2} + \frac{e^{2(k_1+k_2)t}(k_1 - k_2)^4}{4k_1^2 k_2^2 (k_1 + k_2)^4} + \frac{4e^{(k_1+k_2)t}\cos[(k_1^2 - k_2^2)z]}{(k_1 + k_2)^2}. \tag{10c}$$

The intensity of q_j can be explicitly expressed as

$$|q_j|^2 = \frac{e^{2k_1 t}Q_1^2 + e^{2k_2 t}Q_2^2 + 2e^{(k_1+k_2)t}Q_1 Q_2 \cos[(k_1^2 - k_2^2)z]}{4k_1^4 k_2^4 (k_1 + k_2)^4 D^2}. \tag{11}$$

With those considerations, the soliton pulses in the two modes have the identical intensity, which hold the periodic behaviors with the period $T = 2\pi/|k_1^2 - k_2^2|$ along the propagation distance. The investigation on the intensities of the pulses can be carried out for a series of values of k_1 and k_2 by dividing them into several groups of conditions.

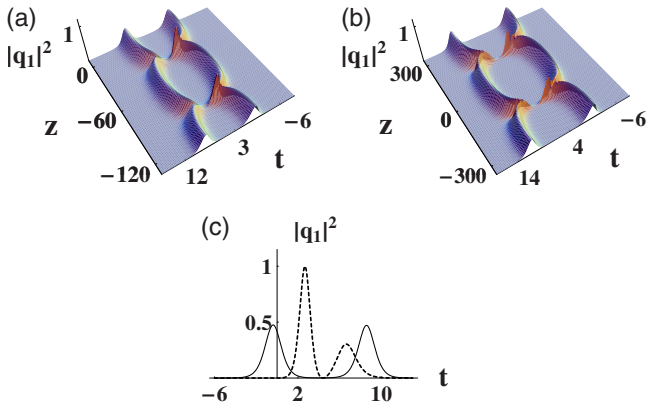

FIG. 1. (Color online) (a) Intensity plots of the bound vector solitons via Eq. (11) for $k_2=0.95$; (b) intensity plots of the bound vector solitons via Eq. (11) for $k_2=0.99$; (c) for $k_2=0.95$, the intensity profile of pulse at $z=0$ (solid line) and $z=32.2$ (dashed line).

A. $k_1=1$ and $0<k_2\leq 1$

Under such choices of the real wave numbers, the two-soliton solutions evolve into certain periodic bound vector solitons. Those structures are sensitive to the degree that k_2 approaches to k_1. When $k_1=k_2=1$, the vector solitons degenerate to the one-soliton solutions; however, if the case of the narrow-banded wave numbers is considered, i.e., $k_2\sim 1$, they exhibit the stationary vector-soliton structures with the periodic attraction and repulsion.

1. $k_2=0.95$ and $k_2=0.99$

As we know, the Kerr solitons interact like real particles, exerting attraction and repulsion on one another [21]. For two equivalent Kerr solitons on initially parallel trajectories, they attract each other in the in-phase case such that they collide periodically along the fiber length [1,21]. In our discussions, the periodic attraction and repulsion for the bound vector solitons exist visibly near the range of $k_2=0.8\sim 1.0$ (not including 1.0). Figures 1(a) and 1(b) illustrate the intensity maps of mode q_1 (mode q_2 has the same form) for $k_2=0.95$ and $k_2=0.99$. In the case of $k_2=0.95$, the maximum separation distance between the peaks of two pulses [corresponding to the solid line in Fig. 1(c)] is $\Delta d_{max}=8.95$ at $z=nT$ $(n=0,\pm 1,\pm 2,\ldots)$, while the minimum distance (dashed line) is $\Delta d_{min}=3.96$ at $z=(1/2+n)T$ $(n=0,\pm 1,\pm 2,\ldots)$. During the attraction process, the energy is transformed from the right pulse to the left one [see Fig. 1(c)] without energy lost for the existence of the integral quantity (2). The asymmetry of the pulse interaction is possibly generated by the slight difference between the two initial pulses at $z=0$. Comparing with the case of $k_2=0.95$, $k_2=0.99$ results in both increase of Δd_{max} and Δd_{min}, namely, 12.03 and 4.59. At the same time, the period has enhanced 3.9 times (from 64.44 to 315.74). Such growth in Δd_{max}, Δd_{min}, and T indicates the corresponding decrease in the strength of the force between the two pulses in the bound state.

2. $k_2=0.5$

When k_2 varies in the range of approximate $0.2\sim 0.8$, the initial two pulses gradually form a stationary soliton complex structure. In such case, parts of the two-soliton pulses are made coherent and the structure behaves as a whole, which is analogical to the PCS [6,13,38]. It can be calculated that the soliton complex with k_2 close to 0.8 (e.g., $k_2=0.7$) has the similar dynamic properties to the one discussed in the last section for its weak coherence. When $k_2=0.5$, the soliton complex provides a symmetry initial pulse at $z=0$ [see Figs. 2(a) and 2(b)] and undergoes an enhancement with two peaks merging into one in a cycle and, spontaneously, the width of the pulse is compressed greatly. The degree of the coherence is increasing with k_2 decreasing (the overlapping of the two basic pulses is enhancing) and the two-peak structure gradually vanishes; however, a completely single structure has not shaped yet [an example can be seen in Fig. 2(c)]. As k_2 approaches to zero, the soliton complex develops to the one-soliton-like structure with intensity periodically enhanced and suppressed.

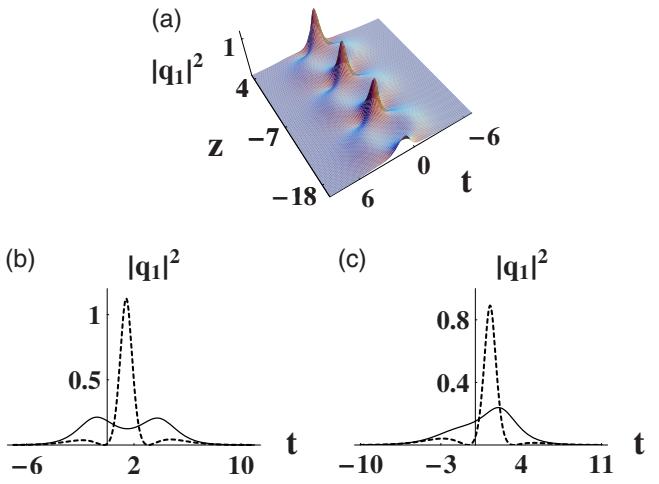

FIG. 2. (Color online) (a) Intensity plots of the soliton complex via Eq. (11) for $k_2=0.5$; (b) for $k_2=0.5$, the intensity profile of pulse at $z=0$ (solid line) and at $z=4.19$ (dashed line); (c) for $k_2=0.36$, the intensity profile of pulse at $z=0$ (solid line) and at $z=3.61$ (dashed line).

We point out that those structures provide the features of the extraordinary high intensities (or saying high power). Taking Figs. 2(b) and 2(c), for example, the amplitude amplifications at half of the cycle can be considerably remarkable (the third times greater than the amplitudes at $z=0$); meanwhile, the amplification happens on a shorter scale in z with k_2 decreasing in the range of $0.2\sim 0.8$. In fact, the soliton complexes in Fig. 2 can be interpreted as the nonlinear superpositions of two one-soliton solutions and the large amplitudes are induced by the interactions of the basic waves. As the nonlinear amplification greatly improves the intensity of the input pulse in such a situation, it is expected that real applications would be possible in the relevant physical systems, especially for the optical fibers and experiments in BECs.

3. $k_2=0.15$

A breatherlike [39] soliton complex with the periodic oscillation (alternate compression and expansion) arises when k_2 approaches to zero, strictly speaking, within the range of

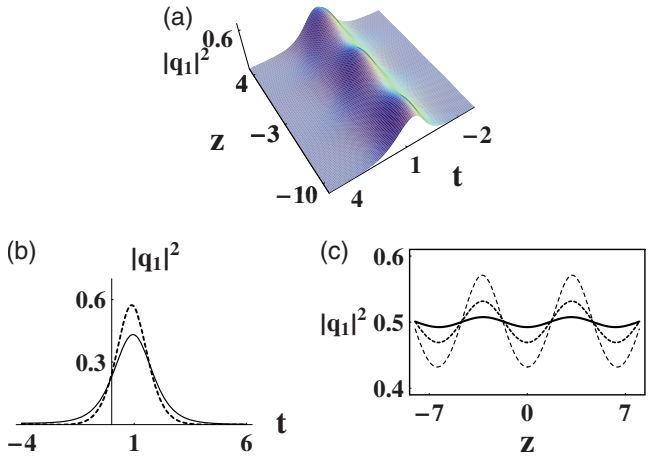

FIG. 3. (Color online) (a) Intensity plots of the soliton complex via Eq. (11) for $k_2=0.15$; (b) for $k_2=0.15$, the intensity profile of pulse at $z=0$ (solid line) and at $z=3.21$ (dashed line); (c) intensity profiles of the soliton complexes at $t=0$ for $k_2=0.05$ (solid line), 0.10 (bold dashed line), and 0.15 (dashed line), respectively.

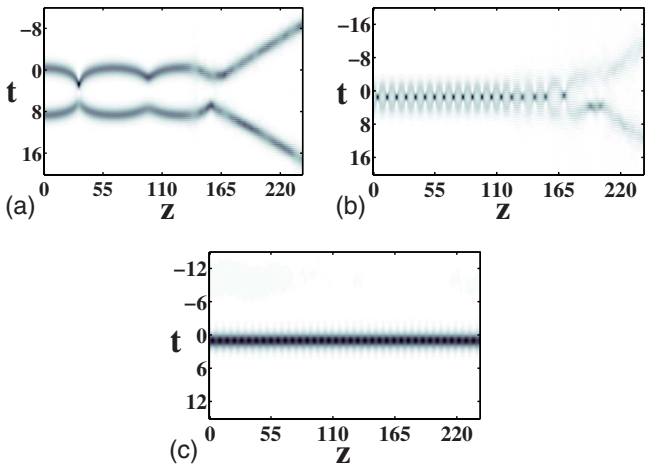

FIG. 4. (Color online) Numerical simulations of the propagations of the initial pulses $q_j(0,t)$, $j=1,2$, for $k_1=1$ and (a) $k_2=0.95$; (b) $k_2=0.5$; (c) $k_2=0.15$.

approximate $0\sim0.2$ ($k_2=0$ corresponds to the complete one-soliton solution). The amplitudes and widths of both components change in a cycle, while the period T varies not much for three groups of k_2 [see Fig. 3(c)], namely, 6.30, 6.35, and 6.43. The maximum decrease in the full width at half maximum (FWHM) in one cycle can be used to describe the compression degree for the pulse. For instance, when $k_2=0.15$ [see Figs. 3(a) and 3(b)], the FWHM of the intensity profile at $z=0$ (solid line) is 1.99, while the one at $z=T/2=3.21$ (dashed line) is 1.59, so the decrease is $\Delta d_{\mathrm{FWHM}}=0.40$. Also Δd_{FWHM} for $k_2=0.10$ and $k_2=0.05$ are 0.18 and 0.04, and the absolute values of the FWHM at $z=0$ vary not much (1.86 for $k_2=0.10$ and 1.78 for $k_2=0.05$), which implies that the degrees of the compression and expansion for the soliton complex pulses in one cycle are weakening with k_2 approaching to zero.

4. Brief numerical simulations of the basic bound vector solitons and soliton complexes

The above three sorts of structures are discussed by virtue of the analytical solutions obtained with the Hirota bilinear method. In this part, numerical simulations are performed to support the results. For Eqs. (1), we use the SSF method [1] to carry out the numerical simulations with the initial vector pulses q_j, $j=1,2$, at $z=0$ (the simulation is proceeded in the MATLAB software environment). Figure 4 presents the numerical results for the above-discussed situations, namely, for $k_2=0.95$, 0.5 and 0.15. The computational domain for t is chosen as $[-25,25]$ and 500 grid points are used. The propagation distance is taken as 250 with a step size of 0.05. In the case of $k_2=0.95$, the pulse propagates in half a cycle consistently with the analytic one [see Fig. 4(a)], and in the second cycle the two pulses in the bound state are not able to achieve the minimum separation distance. During the second half of the third cycle, the energy is dispersed gradually from the bound state, and the two pulses depart from each other after approximately $z\geq160$, which is triggered by the numerical errors. When $k_2=0.5$ [see Fig. 4(b)], the energy of the soliton complex begins to disperse after approximate 11.5 cycles. Regarding $k_2=0.15$, Fig. 4(c) illustrates that the breatherlike structure propagates stably for the whole distance. Further simulations imply that for the given step size along z direction, the initial pulse with k_2 approaching to zero (i.e., the soliton complex with more compact structure) can propagate for a longer distance. One can consider that the multiple bound solitons with the minimum distance between the separated centers of the solitons are most stable, and the situations from Figs. 4(a)–4(c) indeed show the increasingly strengthened bound states with similarity. If more grid points are used in the numerical simulations for the distance z (step size decreasing to 0.01), the propagations of the pulses for above three typical values of k_2 accord with the analytic ones completely within the distance of 250, which indicates the stabilities of those structures.

B. $k_1=1$ and $-1<k_2<0$

The transition of k_2 from positive to negative values brings some new features for the pulse propagations. When k_2 varies in the range of $-0.2\sim0$, the situations are similar to that for the range of $0\sim0.2$ and the single pulse exhibits periodic compression and expansion. As k_2 gradually enters into the range of $-0.8\sim-0.2$, we observe that a part of energy existing as a weakly periodic pulse splits from the single one.

Figures 5(a) and 5(b) describe the pulse propagation when $k_2=-0.5$, from which we notice that a part of pulse with almost no oscillation has been split from the periodic one. The relative enhancement of the amplitude for the left part [see Fig. 5(b)] in a cycle has nonmonotone variation with k_2 in the range of $-0.8\sim-0.2$. To clarify this issue, we denote the largest amplitude of the oscillating part [i.e., the left part in Fig. 5(b)] as $|q_1|^2_{c,max}$ at half of the cycle (dashed line) and the minimum amplitude of that as $|q_1|^2_{e,min}$ (solid line). For a given k_2, $\lambda=(|q_1|^2_{c,max}-|q_1|^2_{e,min})/|q_1|^2_{e,min}$ can be used to describe the relative enhancement of the amplitude of the os-

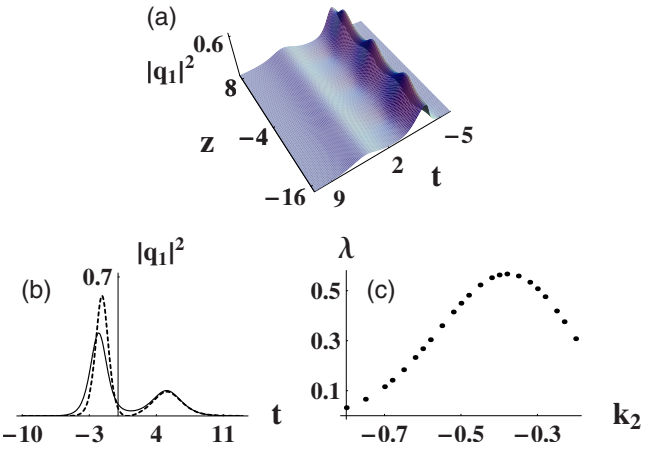

FIG. 5. (Color online) (a) Intensity plots of the soliton complex via Eq. (11) for $k_2=-0.5$. (b) For $k_2=-0.5$, the intensity profile of pulse at $z=0$ (solid line) and at $z=4.19$ (dashed line). (c) Plots of the variation in λ with k_2.

cillating part in one cycle. Figure 5(c) presents the variation of λ with k_2, which indicates that the process consists of two monotone increasing and decreasing phases. When $k_2\sim-0.38$, λ reaches to the maximum value ~0.57, i.e., the maximum amplitude in one cycle exceeds 1.5 times of the initial one. Another feature is that λ approaches to zero when k_2 approaches to −1 (corresponding to the range of $-0.8\sim-1$) and such k_2 provides the two parallel peaks propagating with almost no periodic oscillations (or can be neglected relatively). It is known that in a parallel polarized soliton transmission system, the maximum transmission distance is influenced by the distance of soliton coalescence [40], so the structure with k_2 approaching to −1 might offer a two-peak pulse suitably for the long-distance transmission.

C. $k_1=1$ and $k_2<-1$ or $k_2>1$

When $k_2<-1$ or $k_2>1$, the similar discussions can be addressed, which exhibit the periodic variations in the intensity $|q_1|^2$ more sharply than that in Secs. III A and III B. The range of approximate $1\sim1.25$ for k_2 corresponds to the bound vector solitons, while $1.25\sim3.6$ and $k_2>3.6$ correspond to the analogous soliton complexes in Figs. 2 and 3, respectively. (Note that the structures vary continuously with k_2 increasing, so there are no remarkable critical values to divide the range of k_2 into absolutely distinct regions.) Within the range of $-1.25\sim-1$ for k_2, the situation is just similar to that for $-1\sim-0.8$ and the soliton complex structure for $-1.5\sim-1.25$ can be described in the approximate way for $-0.8\sim-0.2$.

As k_2 varies in the range of $-3\sim-1.5$, the two peaks are gradually emerging into one structure. Especially for k_2 approaching to −1.5, a part of energy is separated from the single one with periodic variation, which is different from the pulse discussed in Sec. III B. Ulteriorly, the pulse similar to the one in Fig. 3, with greater compression and expansion in one cycle, can be derived when $k_2<-3$ approximately. Such large-scope oscillation of the pulse is mainly resulted by the larger deviation of the absolute values of k_1 and k_2.

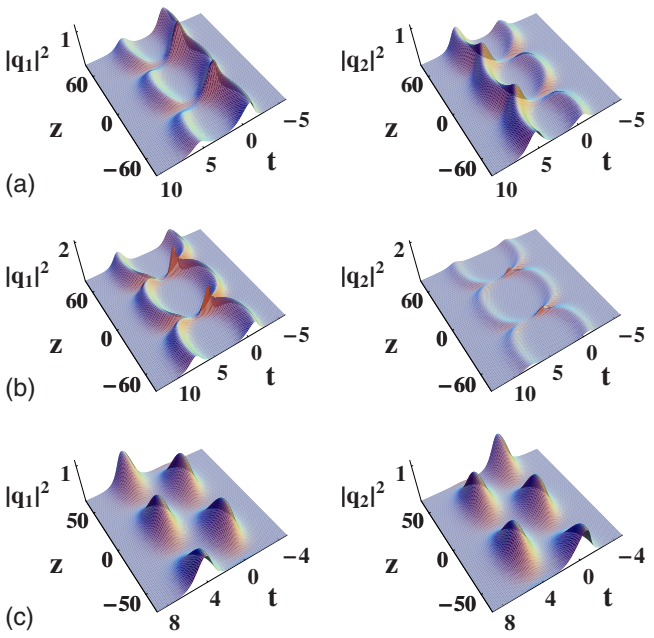

FIG. 6. (Color online) Intensity distributions of the bound vector solitons and soliton complexes in two modes for (a) $k_1=1$, $k_2=0.95$, $\alpha_1^{(1)}=2$, and $\alpha_2^{(1)}=\alpha_1^{(2)}=\alpha_2^{(2)}=1$; (b) $k_1=1$, $k_2=0.95$, $\alpha_1^{(1)}=\alpha_2^{(1)}=2$, and $\alpha_1^{(2)}=\alpha_2^{(2)}=1$; (c) $k_1=1$, $k_2=0.95$, $\alpha_1^{(1)}=-1$, and $\alpha_2^{(1)}=\alpha_1^{(2)}=\alpha_2^{(2)}=1$.

IV. INTENSITY DISTRIBUTIONS OF THE BOUND VECTOR SOLITONS AND SOLITON COMPLEXES IN TWO MODES

For the regular multisolitons of Eqs. (1) (the relative distance between each two single solitons approaches to infinity when $z\to\pm\infty$), the soliton collisions with the shape changing permit different possibilities of energy redistributions among the different modes of solitons [6,11,13,24]. The free parameters $\alpha_1^{(j)}$, $\alpha_2^{(j)}$, $j=1,2$, in Solutions (7) and (8) have direct connections with the collision patterns. For example, $\alpha_1^{(1)}/\alpha_2^{(1)}=\alpha_1^{(2)}/\alpha_2^{(2)}$ gives the elastic collision, while types of inelastic cases (associated with the enhancement and suppression of the pulses) occur for other choices of those parameters. In this section, several cases of the bound vector solitons and soliton complexes with different intensity distributions have been provided and interpreted.

A. Intensity distributions of the bound vector solitons

Figures 6(a) and 6(b) show two asymmetric cases for the bound vector-soliton interactions with the different choices of parameters in the analytical solutions (7) and (8). The first case [see Fig. 6(a)] is a periodical enhancement of the intensity of the right soliton in mode q_1 and suppression of the corresponding soliton in mode q_2 in a cycle, while the left one in both modes has undergone the opposite process. Differently, in the other case [see Fig. 6(b)], the enhancement in one cycle occurs in the right soliton for both modes. From the view of energy switching, most of the total energy in Fig. 6(a) is distributed in the right soliton of mode q_1 and the left soliton of mode q_2 nearly equally, and the total energy of the

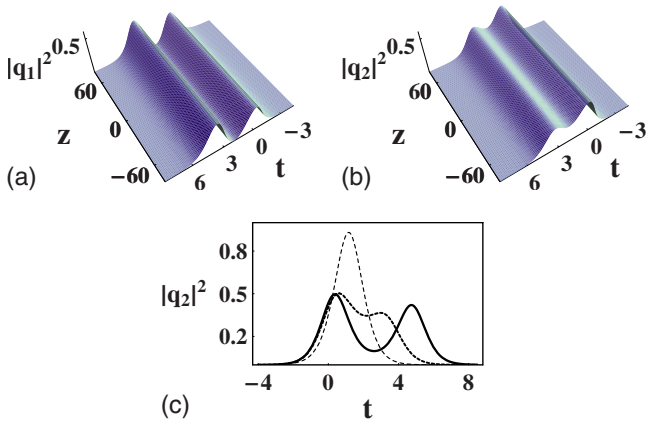

FIG. 7. (Color online) Soliton complexes with $k_1=1$, $k_2=0.85$, $\alpha_1^{(1)}=\alpha_2^{(2)}=0$, and $\alpha_2^{(1)}=\alpha_1^{(2)}=1$ in (a) mode q_1; (b) mode q_2; (c) intensity profiles of the soliton complex in mode q_2 for $k_2=0.95$ (solid line), 0.8 (bold dashed line), and 0.3 (dashed line), respectively.

individual solitons (the right and left ones) in two modes remains approximately equal. As comparison, Fig. 6(b) allows the energy to distribute mainly in one mode (mode q_1). For a cycle in both modes, the energy is concentrated in one soliton (the right one) during the attraction process. Such different behaviors are connected with the parameters $\alpha_1^{(j)}$, $\alpha_2^{(j)}$, $j=1,2$, which have the abilities to control the intensity distributions of both solitons in the bound state for each single mode exactly.

B. Intensity switching of the soliton pulses

As we know, in the case of the two-mode (two-core) fibers with the anomalous group-velocity dispersion, the entire soliton pulse can switch from one mode to another, and such nonlinear switching behaviors have been applied in the ultrafast logic gates using asymmetric fiber couplers [41]. Figure 6(c) has provided two parallel soliton pulses with the energy switching properties. In such case, the left and right pulses, respectively, switch between the two modes completely with the period $T=64.44$, and such period can be controlled by the appropriate choices of k_1 and k_2. Further, the total energy can be distributed in asymmetric manners for either of the pulses if the parameters $\alpha_1^{(j)}$, $\alpha_2^{(j)}$, $j=1,2$ are well selected. One point associated with the integrity of Eqs. (1) is the invariation in the total energy E for the system despite of various possibilities of the intensity distributions.

C. Soliton complexes without periodic interactions

If some of $\alpha_1^{(j)}$, $\alpha_2^{(j)}$, $j=1,2$ are supposed to be zero, a type of soliton complexes can be derived, which have the analogous shapes with the PCS discussed in Refs. [12,32–34]. Figures 7(a) and 7(b) illustrate the soliton complex structures in two modes, in which the coherence is found different between mode q_1 and q_2. The overlapping of the two humps in mode q_2 is more visible than that in mode q_1. When the value of k_2 decreases, more proportion of the total energy is concentrated in mode q_2, and the two-hump soliton complex gradually evolves into a single soliton with the intensity enhanced [the sketch map of evolution can be seen in Fig. 7(c)]. The one in the remaining mode is suppressed correspondingly, with the two-hump structure still obviously visible. If k_2 approaches to zero, almost all energy has switched to mode q_2, forming a one-soliton-like structure; synchronously, the profile of intensity nearly vanishes in mode q_1.

V. COLLISION-INDUCED SHAPE TRANSFORMATIONS OF THE BOUND VECTOR SOLITONS AND SOLITON COMPLEXES

A series of studies have shown that collisions allow the profiles of certain PCS to remain stationary but cause their shapes to change [12,33–35]. In this section, several interesting collision behaviors of the bound vector solitons and soliton complexes will be investigated by choosing the appropriate parameters for the three bright solitons of Eqs. (1). The features of those collisions originate from the shape transformations associated with the intensity redistributions but have more sophisticated presentations.

The analytical three-soliton solutions of Eqs. (1) by the bilinearization procedure have been given in Refs. [13,24], which are not presented here for their trivial details. The complexity of the three-soliton solutions is characterized by 12 complex parameters $\alpha_1^{(j)}$, $\alpha_2^{(j)}$, $\alpha_3^{(j)}$, $j=1,2,3$, k_1, k_2, and k_3. The three wave numbers can be further written as $k_j=k_{jR}+ik_{jI}, j=1,2,3$, where the suffixes R and I represent the real and imaginary parts, respectively. In Sec. III, the typical bound vector solitons and soliton complexes propagating parallel to z have been investigated by the choice of $k_{jI}=0$. In fact, if we set $|k_{jI}| \ll |k_{jR}|$, the propagations of the pulses unparallel to z can be derived and such structures are liable for constructing corresponding collisions with one bright soliton, which attract our interest in the following contents.

A. Collisions of the bound vector solitons and one bright soliton

To the PCS understood as the multisoliton complex, one feature is the reshaping of the soliton with an intensity profile different from the initial one [12,33]. Likewise, Fig. 8 has exhibited the collision-induced shape changing with the intensity redistribution for the bound vector solitons in the two modes. The corresponding parameters for the analytical three-soliton solutions have been given in the captions. In Fig. 8(a), the regular one soliton gets suppressed and the energy is transformed into the asymmetric bound vector solitons during the collision, which induces the formation of the parallel soliton pulses with intensity switching in mode q_1. The situation in its coupled mode q_2 is another image, which shows that the bound vector soliton with the opposite symmetry splits part of its energy to the one soliton and changes into the similar intensity-switching pulses, while the corresponding one soliton is enhanced. To those cases, we can also say that the collision leads to the transformation between the basic patterns studied in Figs. 6(a) and 6(c). Such transformation requires the extra energy input and output,

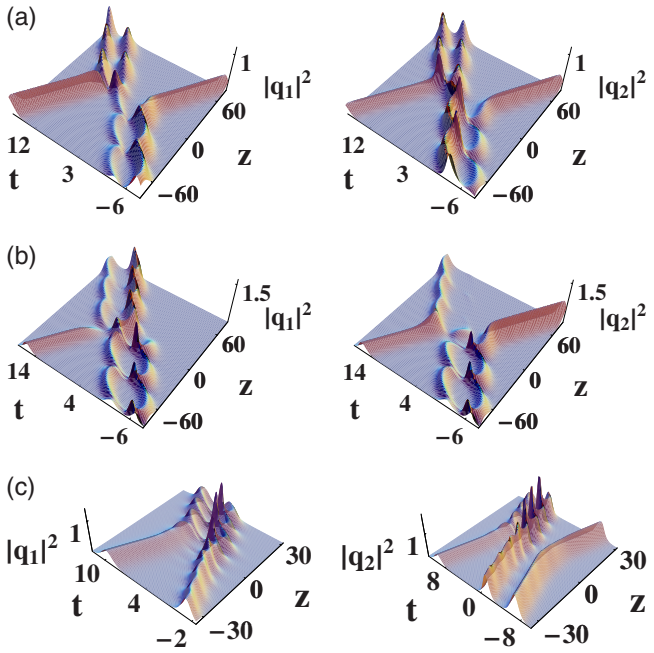

FIG. 8. (Color online) Collisions of the bound vector solitons and one bright soliton for (a) $k_1=0.9+0.05i$, $k_2=1+0.05i$, $k_3=0.9-0.05i$, $\alpha_1^{(1)}=2$, and $\alpha_2^{(1)}=\alpha_3^{(1)}=\alpha_j^{(2)}=\alpha_j^{(3)}=1$, $j=1,2,3$; (b) $k_1=0.9+0.05i$, $k_2=1+0.05i$, $k_3=0.9-0.05i$, $\alpha_3^{(1)}=0$, and $\alpha_1^{(1)}=\alpha_2^{(1)}=\alpha_j^{(2)}=\alpha_j^{(3)}=1$, $j=1,2,3$; (c) $k_1=-1.3+0.05i$, $k_2=1+0.05i$, $k_3=0.9-0.05i$, $\alpha_1^{(1)}=0$, and $\alpha_2^{(1)}=\alpha_3^{(1)}=\alpha_j^{(2)}=\alpha_j^{(3)}=1$, $j=1,2,3$.

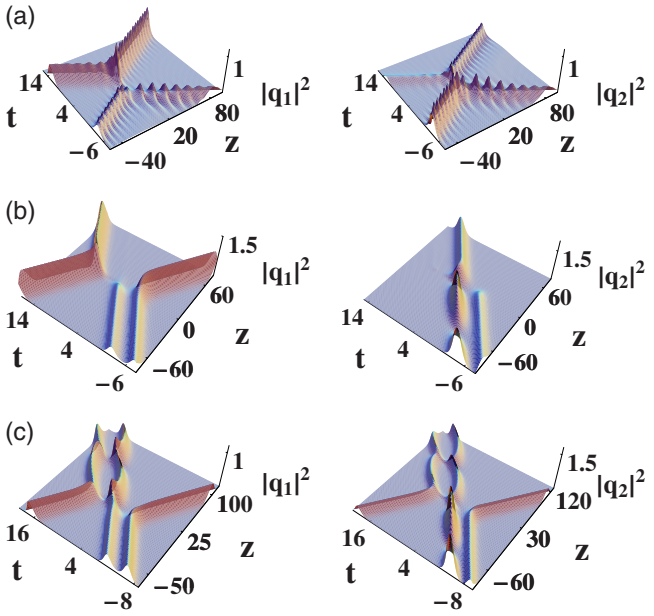

FIG. 9. (Color online) Collisions of the soliton complexes and one bright soliton for (a) $k_1=0.25+0.05i$, $k_2=1+0.05i$, $k_3=0.8-0.05i$, $\alpha_1^{(1)}=2$, and $\alpha_2^{(1)}=\alpha_3^{(1)}=\alpha_j^{(2)}=\alpha_j^{(3)}=1$, $j=1,2,3$; (b) $k_1=0.95+0.05i$, $k_2=1+0.05i$, $k_3=0.95-0.05i$, $\alpha_1^{(1)}=\alpha_2^{(2)}=\alpha_3^{(2)}=0$, and $\alpha_2^{(1)}=\alpha_3^{(1)}=\alpha_1^{(2)}=\alpha_j^{(3)}=1$, $j=1,2,3$; (c) $k_1=0.95+0.05i$, $k_2=1+0.05i$, $k_3=0.95-0.05i$, $\alpha_1^{(1)}=\alpha_2^{(2)}=0$, and $\alpha_2^{(1)}=\alpha_3^{(1)}=\alpha_1^{(2)}=\alpha_3^{(2)}=\alpha_j^{(3)}=1$, $j=1,2,3$.

respectively, in modes q_1 and q_2, which are achieved through the suppression and enhancement of the regular one soliton.

Figure 8(b) provides us with the collision, in which the energy redistribution leads to the increase in the asymmetry for the bound vector solitons. For mode q_1, the regular one soliton completely merges into the bound state, inducing the obvious enhancement of the intensity profile of the right pulse in the bound state, but without transformation of the basic patterns happening in Fig. 8(a). For mode q_2, the energy of the right pulse of the bound vector solitons is taken away by the regular one soliton during collision, leaving only the left one propagating periodically. The enhancing and vanishing both occur to the right pulse for the reason of the slight difference between the real parts of the wave numbers k_1 and k_2.

The first map in Fig. 8(c) illustrates the transformation from the one soliton and breatherlike soliton complex to the bound vector solitons in mode q_1. In mode q_2 (see the second map), the two pulses in the bound state are close to the structure in Fig. 7(a), with weakly periodic compression and expansion. When it collides with the regular one soliton, part of its energy is given to the one soliton, inducing corresponding enhancement for the latter one, and the rest forms a typical bound vector solitons.

The above examples tell us that for the collisions of the bound vector solitons comparing with those of the regular three solitons, not only the enhancement and suppression of the intensity profiles (which may lead to the increase in the asymmetry of the pulses in the bound state), but also the transformations of the basic soliton patterns happen due to the shape changing with the intensity redistribution.

B. Collisions of the soliton complexes and one bright soliton

In this part, our interest will be devoted to the collisions of the basic soliton complexes discussed in Figs. 3 and 7. As interpreted previously, the analysis is based on the analytical three-soliton solutions. Figure 9(a) shows the collision between the breatherlike soliton complex and regular one soliton in the two modes, in which the two structures are well separated before and after collision. In mode q_1, the soliton complex gets enhanced in its amplitude, while the regular one soliton is suppressed after collision. Interestingly, the different changes are observed in mode q_2, where the soliton complex gets suppressed and the one soliton is enhanced. The scenario of the intensity redistributions is similar to that for the collision of the regular two solitons in the Manakov system [6,27]. Specially, for the case of $\alpha_j^{(1)}=\alpha_j^{(2)}=\alpha_j^{(3)}=1$, $j=1,2,3$, the elastic collision between the soliton complex and regular one soliton occurs without shape changing. Another attractive phenomenon in the finite collision region is that the breatherlike soliton complex induces the one soliton to exhibit oscillation in shape for several cycles, and such effect disappears gradually with the separation distance increasing. Reference [27] has mentioned the concept *controlling the switching dynamics*, referring to the suppression and enhancement of the periodic oscillations in the energy switching process completely or partially. Their way is to use the collision between two oscillations. Here the enhancement and compression of the breatherlike soliton complexes in

Figs. 9(a) and 9(b), respectively, can also be controlled by appropriately choosing the parameters, and such controls are mainly partial in the present study. Further, our way is based on the collision between the breatherlike soliton complex and regular one soliton as difference.

The two incoherent humps of the soliton complex can merge into one hump, forming a regular one soliton in mode q_1 through collision, which is shown in Fig. 9(b). Correspondingly in its coupled mode q_2, the mergence occurs between the one soliton and breatherlike soliton, leading to the formation of the one soliton with enhanced amplitude. In other words, the breatherlike soliton is completely suppressed during the interaction. Mergence is not the only pattern that such soliton complex undergoes during collision; the formation of the bound vector solitons after collision is shown in Fig. 9(c) as another image. In such a condition, unlike the automergence in mode q_2 shown in Fig. 9(b), the formation of the bound vector solitons in the same mode in Fig. 9(c) is induced by the collision with the regular one soliton.

The above descriptions of the collisions of the bound vector solitons or soliton complexes demonstrate some unique shape-changing phenomena associated with the intensity redistributions comparing with those for the regular multisolitons. Since 12 free complex parameters are provided in the explicit three-soliton solutions, more collision behaviors with interpretations can be derived by controlling those parameters, which will be treated in a future publication.

VI. CONCLUSIONS

In this paper, we have studied the bound vector solitons and soliton complexes for Eqs. (1) by the different choices of the arbitrary parameters for the multisoliton solutions. Shape transformation with energy redistribution for the regular vector multisolitons has been employed to explain the corresponding phenomena for those stationary structures illustrated in Figs. 1–9. Results have been both supported by the analytical solutions obtained with the Hirota bilinear method [36] and numerical procedure with the SSF method [1].

In the classification of various stationary structures, two categories of energy transformation patterns during soliton interactions have been exhibited (see Figs. 1–4), namely, the periodic transformation between the two pulses and self-oscillation (compression and expansion for one pulse). Formation of the stationary structures with different coherence has close relationship with the separation distance between the initial two pulses at the propagation distance $z=0$. For the case of periodic attraction and repulsion (see Fig. 1), the interaction period along the propagation distance increases with the separation distance increasing (or with the two wave numbers approaching to each other). In the parallel soliton transmission system, such feature could be used to avoid the interference caused by the collision when the interaction distance in one period is controlled to be longer than the transmission distance. With the coherence of the two pulses enhanced, the energy can be confined in a small region within a cycle, which induces the appearance of the extraordinary high intensity (see Fig. 2). Self-oscillation occurs as the two wave numbers deviating from each other (see Fig. 3). If one wave number approaches to zero, the oscillation becomes very weak [see Fig. 3(c)], which provides a path to suppress the interaction with very strong coherence. Numerical simulations have revealed that the two-soliton pulses with stronger coherence can propagate more stably, as seen in Fig. 4. On the other hand, those discussions have revealed a fact that the basic interaction patterns can be controlled by the initial conditions of the two pulses at $z=0$, which is similar to that presented in the introduction for the regular vector solitons.

Our investigations have exactly indicated that the total energy can be distributed asymmetrically between the individual pulses in the bound state for the same mode [see Fig. 6(a)] or between the single modes [see Fig. 6(b)]. For the former case, the interaction in each single mode happens closely to the pulse with the higher intensity of the two during a period. For the latter case, there exists the similarity between the interactions in both modes despite the unequal energy distribution for each single mode.

Other features we can derive involve the two parallel soliton pulses with the periodic energy switching between the two modes [see Fig. 6(c)] and overlapped two-hump soliton complexes without the periodic interactions (see Fig. 7). The former can be viewed as the complicated condition for the case of the single pulse. The latter provides us with the coherent structure in which the periodic interaction between the two humps is completely suppressed. Generally speaking, the generation of those two structures is attributed to the choice of the negative or zero values for the parameters $\alpha_1^{(j)}$, $\alpha_2^{(j)}$, $j=1,2$, partially.

Collision-induced shape changing of the bound vector solitons and soliton complexes has been investigated in this paper. Some of the structures discussed above can be changed when they collide with the regular one soliton. Moreover, with the regular one soliton suppressed (enhanced) during the collisions, the energy input (output) into the bound vector solitons may induce the following two effects depending on the parameters: (i) the asymmetric increase or decrease in the pulses in the bound state for each mode [see Fig. 8(b)]; (ii) the transformation of the basic soliton patterns according to the classifications in Sec. III [see Figs. 8(a), 8(c), 9(b), and 9(c)]. Those behaviors have direct connections with the shape changing (intensity redistribution) of the three-soliton collisions. In other words, both effects depend on how the energy is redistributed between the one soliton and stationary structure during the collision process.

Additionally, the result has been exactly obtained that the scenario of the intensity redistributions for the regular multisolitons in the Manakov system [27] can be applied to enhance or suppress the breatherlike soliton complex partially [see Fig. 9(a)]. Such breatherlike soliton complex is strongly coherent so as to make it behave like a single soliton during the collision. Therefore, another route has been supplied to suppress the oscillation for the breatherlike soliton complex by taking its energy away during the collision. Also, the collision-induced transformation of the overlapped two-hump soliton complex into the one soliton or into the bound

state has been studied simultaneously. Essence of the transformation can be concluded as the effect of energy redistribution as mentioned above.

In conclusion, the two questions mentioned in the introduction have been solved to some extent. Energy redistribution has been investigated and such behavior for the fundamental solitons can be used to explain the interaction of the stationary structures. Those discussions could be expected to be helpful in describing the pulse propagations and providing the relevant applications in the multimode nonlinear fiber optics and BECs. As another aspect, the bound vector solitons and soliton complexes in the nonlinear fiber optics give the simplified and analogous pictures of the corresponding structures in other systems governed by the CNLS equations, e.g., the dynamics of coupled nonlinear waves in the plasma physics and BECs.

ACKNOWLEDGMENTS

We express our sincere thanks to the editors and referee for their valuable suggestions. We are also very grateful to all the members of our discussion group for their beneficial comments. This work has been supported by the National Natural Science Foundation of China under Grant No. 60772023, by the Open Fund of the State Key Laboratory of Software Development Environment under Grant No. BUAA-SKLSDE-09KF-04, Beijing University of Aeronautics and Astronautics, by the National Basic Research Program of China (973 Program) under Grant No. 2005CB321901, and by the Specialized Research Fund for the Doctoral Program of Higher Education (Grants No. 20060006024 and No. 200800130006), Chinese Ministry of Education.

[1] G. P. Agrawal, *Nonlinear Fiber Optics*, 3rd ed. (Academic, San Diego, CA, 2001).
[2] W. P. Hong, Phys. Lett. A **361**, 520 (2007); B. Tian and Y. T. Gao, Eur. Phys. J. D **33**, 59 (2005); Phys. Plasmas **12**, 054701 (2005); **12**, 070703 (2005); Phys. Lett. A **340**, 243 (2005); **340**, 449 (2005); **362**, 283 (2007).
[3] G. Das and J. Sarma, Phys. Plasmas **6**, 4394 (1999); Z. Y. Yan and H. Q. Zhang, J. Phys. A **34**, 1785 (2001); Y. T. Gao and B. Tian, Phys. Plasmas **13**, 112901 (2006); **13**, 120703 (2006); Phys. Lett. A **349**, 314 (2006); **361**, 523 (2007); Europhys. Lett. **77**, 15001 (2007); B. Tian, G. M. Wei, C. Y. Zhang, W. R. Shan, and Y. T. Gao, Phys. Lett. A **356**, 8 (2006).
[4] M. P. Barnett, J. F. Capitani, J. Von Zur Gathen, and J. Gerhard, Int. J. Quantum Chem. **100**, 80 (2004); B. Tian, W. R. Shan, C. Y. Zhang, G. M. Wei, and Y. T. Gao, Eur. Phys. J. B **47**, 329 (2005); B. Tian and Y. T. Gao, Phys. Lett. A **342**, 228 (2005); **359**, 241 (2006); B. Tian, Y. T. Gao, and H. W. Zhu, *ibid.* **366**, 223 (2007); K. H. Spatschek, Phys. Fluids **21**, 1032 (1978).
[5] A. Hasegawa and F. Tappert, Appl. Phys. Lett. **23**, 142 (1973).
[6] T. Kanna and M. Lakshmanan, Phys. Rev. Lett. **86**, 5043 (2001).
[7] Y. Kodama and A. Hasegawa, IEEE J. Quantum Electron. **23**, 510 (1987).
[8] S. Chakravarty, M. J. Ablowitz, J. R. Sauer, and R. B. Jenkins, Opt. Lett. **20**, 136 (1995).
[9] C. Yeh and L. Bergman, Phys. Rev. E **57**, 2398 (1998).
[10] A. Biswas, Opt. Quantum Electron. **38**, 605 (2006).
[11] R. Radhakrishnan, M. Lakshmanan, and J. Hietarinta, Phys. Rev. E **56**, 2213 (1997).
[12] N. Akhmediev, W. Królikowski, and A. W. Snyder, Phys. Rev. Lett. **81**, 4632 (1998).
[13] T. Kanna and M. Lakshmanan, Phys. Rev. E **67**, 046617 (2003).
[14] M. Vijayajayanthi, T. Kanna, and M. Lakshmanan, Phys. Rev. A **77**, 013820 (2008).
[15] M. Onorato, D. Ambrosi, A. R. Osborne, and M. Serio, Phys. Fluids **15**, 3871 (2003).
[16] W. Craig, D. M. Henderson, M. Oscamou, and H. Segur, Math. Comput. Simul. **74**, 135 (2007).
[17] M. Onorato, A. R. Osborne, and M. Serio, Phys. Rev. Lett. **96**, 014503 (2006).
[18] P. K. Shukla, I. Kourakis, B. Eliasson, M. Marklund, and L. Stenflo, Phys. Rev. Lett. **97**, 094501 (2006); P. K. Shukla and A. A. Mamun, Phys. Plasmas **11**, 1233 (2004).
[19] P. K. Shukla, M. Marklund, and L. Stenflo, JETP Lett. **84**, 645 (2007); I. Kourakis, P. K. Shukla, and G. E. Morfill, Phys. Plasmas **12**, 082303 (2005); P. K. Shukla, B. Eliasson, M. Marklund, L. Stanflo, I. Kourakis, M. Parviainen, and M. E. Dieckmann, *ibid.* **13**, 053104 (2006).
[20] A. Grönlund, B. Eliasson, and M. Marklund, Europhys. Lett. **86**, 24001 (2009).
[21] G. I. Stegeman and M. Segev, Science **286**, 1518 (1999).
[22] S. V. Manakov, Sov. Phys. JETP **38**, 248 (1974).
[23] R. Radhakrishnan, P. T. Dinda, and G. Millot, Phys. Rev. E **69**, 046607 (2004).
[24] T. Kanna, M. Lakshmanan, P. T. Dinda, and N. Akhmediev, Phys. Rev. E **73**, 026604 (2006).
[25] D. Rand, I. Glesk, C. S. Brès, D. A. Nolan, X. Chen, J. Koh, J. W. Fleischer, K. Steiglitz, and P. R. Prucnal, Phys. Rev. Lett. **98**, 053902 (2007).
[26] C. Anastassiou, M. Segev, K. Steiglitz, J. A. Giordmaine, M. Mitchell, M. F. Shih, S. Lan, and J. Martin, Phys. Rev. Lett. **83**, 2332 (1999).
[27] T. Kanna, M. Vijayajayanthi, and M. Lakshmanan, Phys. Rev. A **76**, 013808 (2007).
[28] M. Haelterman and A. Sheppard, Phys. Rev. E **49**, 3376 (1994).
[29] C. De Angelis and S. Wabnitz, Opt. Commun. **125**, 186 (1996).
[30] A. P. Sheppard and Y. S. Kivshar, Phys. Rev. E **55**, 4773 (1997).
[31] J. Yang, Phys. Rev. E **64**, 026607 (2001).
[32] A. A. Sukhorukov and N. N. Akhmediev, Phys. Rev. Lett. **83**, 4736 (1999).
[33] W. Królikowski, N. Akhmediev, and B. Luther-Davies, Phys.

Rev. E **59**, 4654 (1999).
[34] A. Ankiewicz, W. Królikowski, and N. N. Akhmediev, Phys. Rev. E **59**, 6079 (1999).
[35] N. M. Litchinitser, W. Królikowski, N. N. Akhmediev, and G. P. Agrawal, Phys. Rev. E **60**, 2377 (1999).
[36] R. Hirota, *The Direct Method in Soliton Theory* (Cambridge University Press, Cambridge, 2004).
[37] R. Radhakrishnan and K. Aravinthan, Phys. Rev. E **75**, 066605 (2007).
[38] T. S. Ku, M. F. Shih, A. A. Sukhorukov, and Y. S. Kivshar, Phys. Rev. Lett. **94**, 063904 (2005).
[39] M. Chen, D. J. Kaup, and B. A. Malomed, Phys. Rev. E **69**, 056605 (2004).
[40] S. Chi, C. F. Chen, and J. C. Dung, Opt. Commun. **147**, 42 (1998).
[41] G. P. Agrawal, *Applications of Nonlinear Fiber Optics* (Academic, San Diego, CA, 2001).